www.cafetinnova.org

ISSN 0974-5904, Volume 10, No. 04

DOI:10.21276/ijee.2017.10.0415

International Journal of Earth Sciences and Engineering

August 2017, P.P. 833-843

Numerical Model of Tidal Current for Power Harvesting in Bangka Strait

HARMAN AJIWIBOWO, KANISIUS S. LODIWA, MUNAWIR B. PRATAMA AND ANDOJO WURJANTO

Faculty of Civil and Environmental Engineering, Institut Teknologi Bandung, Bandung 40132, Indonesia

Email: *Harman.ajiwibowo65@gmail.com, sagari.lodiwa@gmail.com, munawirbintang@gmail.com, andojowurjanto@ocean.itb.ac.id*

Abstract: Exploration of renewable energy sources is necessary to discover alternative energy sources in the current context of depleting fossil-based energy. Ocean hydrodynamic components such as tidal current are abundant yet not widely utilized. The current study is aimed at determining a potential site for tidal current power energy using a certain current turbine. The study consists of field measurement, numerical modeling and its validation, and the selection of a potential site. The field measurement was carried out using an Acoustic Doppler Current Profiler (ADCP) type Argonaut-XR. It resulted in ten layers of tidal current data. Numerical modeling was performed using MIKE 3 and validated by the ADCP data. A potential spot in the Province of Bangka Belitung Islands, called the Kelian Cape site, was selected based on its maximum current output and maximum clearance from ship navigation routes. A Verdant Kinetic Hydropower System turbine is selected to harvest the potential power generated by the tidal current and resulted in 3,270.18 kWh per turbine. Although not significant, this nevertheless gives good motivation for ocean-induced energy power harvesting in Indonesia. Further research toward inventing a turbine with a low cut in speed is needed.

Keywords: *Ocean renewable energy, Tidal current, Numerical modeling, Bangka Strait, Indonesia.*

1. Introduction

Global greenhouse gas (GHG) emissions have been growing since pre-industrial times, with an increase of 70% between 1970 and 2004. The largest growth in global GHG emissions between 1970 and 2004 came from the energy supply sector (an increase of 145%). One of the future key mitigation strategies for technologies and practices in the energy supply sector is to develop advanced renewable energy, including tidal and wave energy [1].

In Indonesia, renewable energy such as geothermal-based and hydropower have the highest share, with values close to 3% (1.3 GW) and 10% (5.1 GW) respectively. In addition, other renewable energy power plants (solar, wind, landfill, hydro, and bio-mass) also began to operate with a total capacity of 96 MW [2].

Ocean covers 75% of the Indonesia region, making it a challenge for the nation's engineers to discover potential sites to harvest energy. Wave, tidal and thermal-based power energy have been explored with various degrees of success. Recent studies on wave, tidal, and ocean thermal-based energy harvesting have resulted in energy yields of 1,995 MW, 17,989 MW, and 41,001 MW, respectively [3]. Ocean wave-based energy produces a less significant amount of energy. In addition, technology readiness is still the main constraint of ocean thermal energy. The most reliable ocean renewable energy resource in Indonesia at present is tidal current-based energy.

There are a number of methods to extract electric power from tidal energy. The most recent invention is dynamic tidal power, which is still being developed. The first generation of tidal power extraction methods are tidal barrages, which include walls to create a different head between open and closed water. The second generation is a type of generator that directly converts tidal current into electricity using a turbine in open water. The first generation requires a large tidal range and high investments, especially to build the wall. Thus, the tidal current-based method is the best option in Indonesia at present.

There have been several studies on tidal current energy harvesting around the world. Topics range from the design of devices [4], tidal array arrangement [5], hydrodynamic modeling [6], leasing and phasing study [7], etc.

Recent studies on tidal current energy harvesting in Indonesia show 11 potential locations, in Malacca Strait, Bangka Islands, Sunda Strait, East Java, Bali, East Nusa Tenggara, West Nusa Tenggara, and West Papua [3,8]. In Bangka Island, the potential tidal current-based energy has been assessed locally in Kelabat Bay, but the tidal current along Bangka Strait has not been evaluated [9]. The motivation for the present study is to produce a valid hydrodynamic numeric model and to determine the site which has the highest potential tidal current in Bangka Strait. Moreover, it is used to determine the most suitable turbine and the electrical power that can be extracted.

Received: February 17, 2017; Accepted: June 21, 2017; Published: August 30, 2017
International Journal of Earth Sciences and Engineering, 10(04), 833-843, 2017, DOI:10.21276/ijee.2017.10.0415

2. Study Location

Bangka Strait is located between South Sumatra Province and Bangka Island as shown in Figure 1a. The northern inlet and southern inlet of Bangka Strait are up to 80 km wide and 60 km, respectively. The width of the Strait is between 13 km and 40 km. The study area is located at the north inlet of Bangka Strait, notably around the coastal zone of Kelian Cape (see Figure 1b). The tidal characteristic in Kelian Cape is found to be mixed mainly semidiurnal and the tidal range is around 2.8 m [10].

Moreover, there are three tidal current velocity measurement stations along Bangka Strait which show 1 m/s as the maximum current velocity [11].However, the current velocity at Kelian Cape is anticipated to be greater. Part of the mass from Karimata Strait will be directed to Bangka Strait via the north or the south inlet. The flow is intensified as it comes from Karimata Strait .into Bangka Strait.

3. Field Measurement

Field measurement was conducted to acquire several physical conditions in Bangka Strait, such as the bathymetry, surface elevation, and tidal current velocity. The locations for field measurement were decided based on the logical hypothesis that the highest velocity will be found at the turning and tapering region of Kelian Cape. The specifications of each field measurement will be explained.

3.1 Bathymetry

The bathymetric survey equipment comprised a transducer and a global positioning system (GPS) echosounder. Figure 2 shows the GPS antenna, directly below the water, and right at the bottom of the antenna is the transducer. The bathymetric survey was conducted to provide a base map of an area of 10×10 km^2 of Bangka Strait. The area of the bathymetric survey is shown in Figure 3 by the dotted yellow line. The greatest depth is found to be 50 m.

3.2 Tidal Observation Survey

The tidal survey was carried out by observation using a staff gauge set in a trestle structure in Kelian Cape

Figure 2. *Bathymetric survey activity*

(Figure 4). The location is shown in Figure 3 as S3 (105.133 E, 2.0847 S) and was chosen as it is calm and the depth can be presented for both high and low water conditions. The field data were recorded hourly for a half moon cycle of about 16 days. The data were recorded from 21 December 2013 to 5 January 2014. The tidal analysis using the field data shows that the tidal range is 2.5 m and the tidal type is mixed, mainly diurnal.

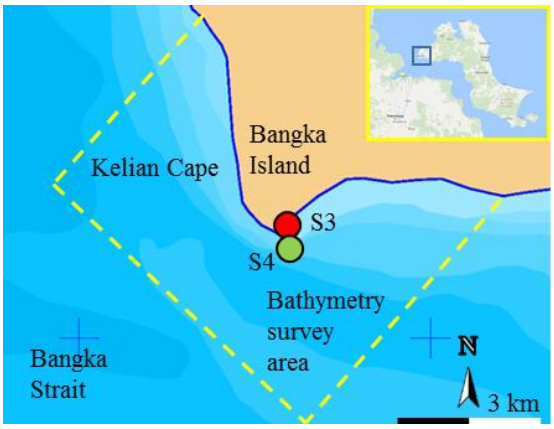

Figure 3. *The area of bathymetric survey and location of surface elevation (S3) and tidal current velocity measurement (S4)*

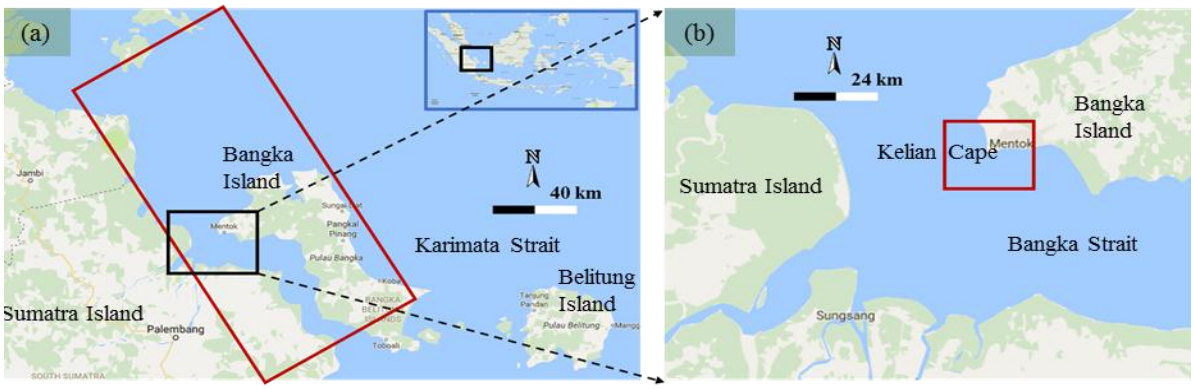

Figure 1. *Location of a) Bangka Island and b) Kelian Cape*

Figure 4. *Tidal observation survey*

3.3 Tidal Current

Figures 5 and 6 show the layers of measurement (10 layers) and placement of the Acoustic Doppler Current Profiler (ADCP). The ADCP is an Argonaut-XR type with a 0.75-MHz autonomous multi-cell system specification. Figure 3 shows the location of field measurement, denoted as S4 (105.1564 E, 2.0902 S). The ADCP was located at a water depth of 20 m. The measured tidal current velocity at S4 ranges from 1.0 to 106.1 cm/s.

The tidal current velocity direction was also known to be dominantly directed to the east when in transition from flood to ebb, while the flow is to the west when the condition is from ebb to flood.

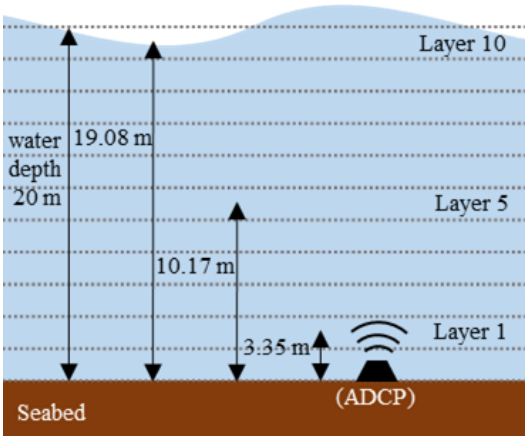

Figure 5. *Illustration of ADCP's layer structure*

Figure 6. *ADCP and the stabilizing steel frame*

4. Numerical Modeling

A numerical model is conducted to provide the distribution of particular parameters at several points at any particular time. The numerical model software has been used previously in various topics, such as tsunami simulation [12], flooding [13], coastal, estuary, and river processes [14], and particle tracking [15].

In this study, the numerical model is addressed to determine the velocity distribution in order to identify the potential site and the power potential of the tidal current velocity. Similar studies have been conducted using other software, such as Delft3D [16], Telemac [6], Regional Ocean Modeling System (ROMS) [17], Finite Volume Community Ocean Model (FVCOM) [18], and MIKE [19]. The current study uses MIKE 3 (personal license).

4.1 Governing Equations

MIKE 3 is a hydrodynamic modeling tool and is already utilized in a wide range of applications around the world. It is based on the finite element method. A three- dimensional hydrodynamic model with sigma coordinates was developed using MIKE 3. The model solves the three-dimensional incompressible Reynolds Averaged Navier–Stokes (RANS) equations using the assumptions of Boussinesq and of hydrostatic pressure [20]. The governing equations of MIKE 3 [20] can be rewritten as Eqs. (1), (2), and (3).

$$\frac{\partial h}{\partial t}+\frac{\partial hu}{\partial x'}+\frac{\partial hv}{\partial y'}+\frac{\partial h\omega}{\partial \sigma}=hS \tag{1}$$

$$\frac{\partial hu}{\partial t}+\frac{\partial hu^2}{\partial x'}+\frac{\partial hvu}{\partial y'}+\frac{\partial h\omega u}{\partial \sigma}= fvh-gh\frac{\partial \eta}{\partial x'}$$
$$-\frac{h}{\rho_0}\frac{\partial p_a}{\partial x'}-\frac{hg}{\rho_0}\int_z^n\frac{\partial \rho}{\partial x}dz-\frac{1}{\rho_o}\left(\frac{\partial s_{xx}}{\partial x}+\frac{\partial s_{xy}}{\partial y}\right) \tag{2}$$
$$+hF_u+\frac{\partial}{\partial \sigma}\left(\frac{v_v}{h}\frac{\partial u}{\partial \sigma}\right)+hu_sS$$

$$\frac{\partial hv}{\partial t}+\frac{\partial huv}{\partial x'}+\frac{\partial hv^2}{\partial y'}+\frac{\partial h\omega v}{\partial \sigma}=-fuh-gh\frac{\partial \eta}{\partial y'}$$
$$-\frac{h}{\rho_0}\frac{\partial p_a}{\partial y'}-\frac{hg}{\rho_0}\int_z^n\frac{\partial \rho}{\partial y}dz-\frac{1}{\rho_o}\left(\frac{\partial s_{yx}}{\partial x}+\frac{\partial s_{yy}}{\partial y}\right) \tag{3}$$
$$+hF_v+\frac{\partial}{\partial \sigma}\left(\frac{v_v}{h}\frac{\partial v}{\partial \sigma}\right)+hv_sS$$

where t is the time; x', y', and σ are the modified Cartesian coordinates; u, v, and w are the velocities in the x', y', and σ axis; h is the total water depth; η is the water level from MSL; f is the Coriolis parameter; g is the gravitational acceleration; p_a is the atmospheric pressure; ρ_0 is the fluid density; v_s is the vertical turbulent viscosity;

s_{xx}, s_{xy}, s_{yx}, and s_{yy} are the radiation stress components; S is the magnitude of point source

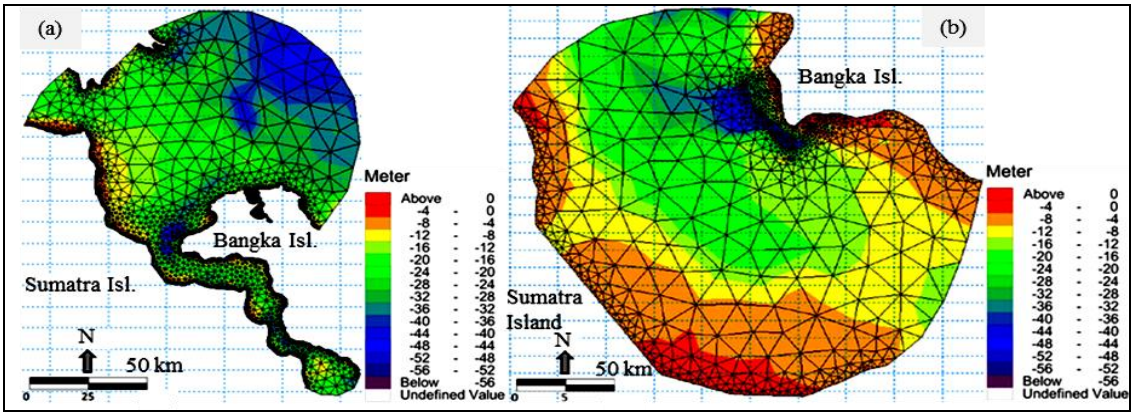

Figure 7. *Domain of a) global model and b) local model*

discharge; Lastly, u_s and v_s are the velocities of the discharge.

4.2 Model Setup

Hydrodynamical modeling is carried out in two stages: global and local. Figures 7a and 1a (red box) show the global model, covering Bangka and Karimata straits. Figures 7b and 1b (red box) show the local model, which covers the area of Kelian Cape. The setup of the global and local domains refers to the model setup in research on the assessment of tidal current power potency in Kelabat Bay [9]. Kelabat Bay is located on the east side of Kelian Cape.

The maximum and minimum global model mesh resolutions are 30 km and 600 m, respectively. The grid becomes finer from the boundary at Karimata and Bangka straits and into the bay. A combination of processed bathymetric survey data and a digitized navigational chart map from the Indonesian Navy is used for modeling. The NaoTide web open application was used to develop the tidal fluctuations at the boundaries of the global model.

The local model has maximum and minimum mesh resolutions of 4.5 km and 280 m, respectively. The local model is created to provide a detailed tidal current velocity model in Kelian Cape, resulting in 11 layers of tide-induced current velocity data output.

4.3 Model Validation

Eq. 4 shows the accuracy level of model validation. Model validation is carried out by comparing the model output with the current velocity obtained from field measurement. Notably in hydrodynamic modeling, the two most common parameters for validation are surface elevation and current velocity [21]. Errors ρ are calculated with a simple formula as shown in Eq. (4), where λ_m is the numerical model result value and λ_{field} is the field measurement data value. μ is the tidal range.

$$\rho = \frac{\left|\lambda_m - \lambda_{field}\right|}{\mu} \quad (4)$$

4.3.1 Surface Elevation Validation

The resulting surface elevations obtained from the global model are validated at locations S1 (Dabosingkep) and S2 (Muntok), as seen in Figure 8. Those hourly data are obtained from the Indonesian Navy database. The model and its validation were carried out in November 2013, as seen in Figures 9a and 9b. Using Eq. (4), the error is about 4.5%, which is sufficient for validation.

The resulting surface elevations obtained from the local model were validated using tidal field measurement at S3 as shown in Figure 10. The validation using 10-minute interval surface data results in 6.2% error, which is relatively good. The validation can be seen in Figure 11.

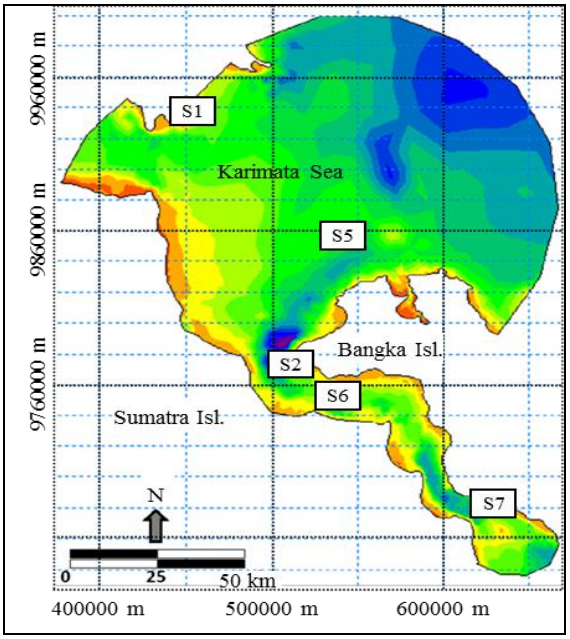

Figure 8*. Validation locations for global model using Indonesian Navy database. The global model validation refers to Ajiwibowo et al (2017) [9]*

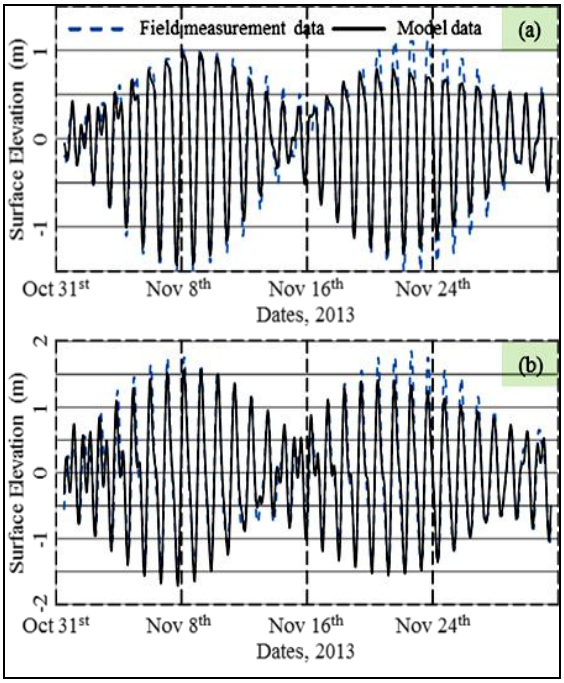

***Figure 9**. Surface elevation validation using data obtained from tidal database of Indonesian Navy: a) S1 and b) S2 [9]*

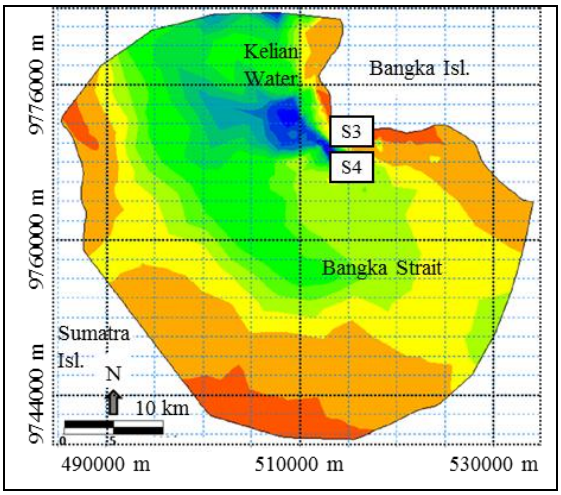

***Figure 10**. Tidal field measurement locations for local model validation, S3 is the surface elevation field measurement location, S4 is the tidal current measurement location*

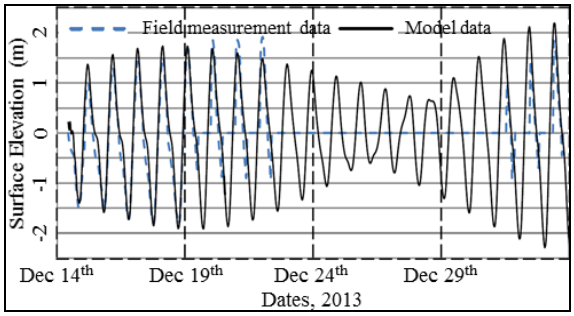

***Figure 11**. Surface elevation validation at S3 at Kelian Cape. Data from field measurement*

4.3.2 Tidal Current Validation

Validation of the tidal current for the global model was conducted at Tujuh Island (S5), Amelia Shoal (S6), and Nemesis Shoal (S7), as seen in Figure 8. These validation data are obtained from the Indonesian Navy data, which comprise the tidal current at the surface. The model results for the uppermost layer are compared with these Indonesian Navy data. Calculation of the error ρ using Eq. (4) results in 8%. Figure 12 shows a good agreement between the model and validation data.

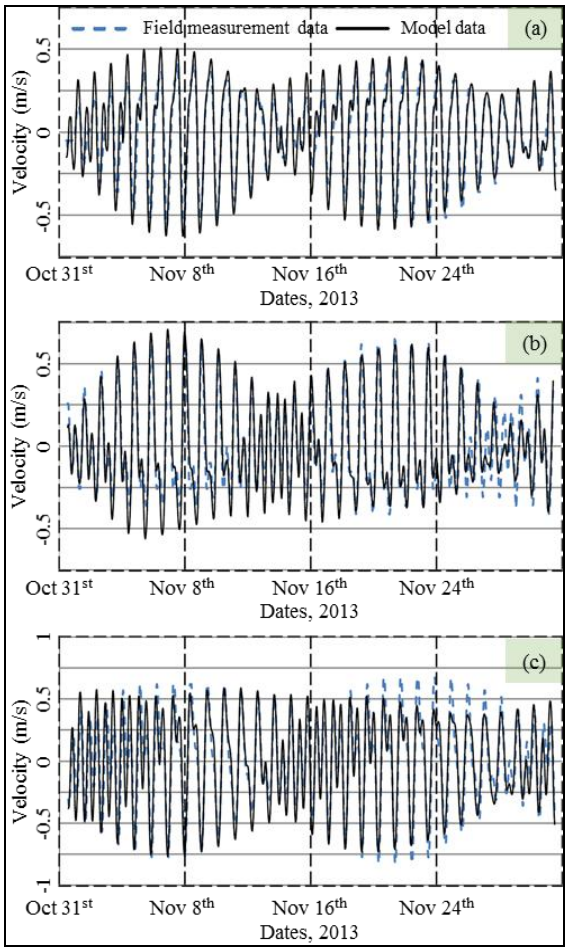

***Figure 12**. Tidal current velocity validation using Indonesian Navy database: a) S5, b) S6, and c) S7*

The local model results were validated using field measurement data at location S4 (see Figure 10). Table 1 shows the validation summary for each layer, and the average error is 12.32%. The results for layer 7 show the smallest error, since this layer is away from the surface and seabed boundaries. The effects of both free surface waves and bed resistance do not interfere with the generation of physical tidal current. Figures 13a and 13b show good agreement between the field data and model result for 10-minute intervals. The validation shown is for layer 7.

***Table 1**. Error result of current velocity validation at Kelian Cape*

Layer	Error S2 (%)
1	14.45
2	14.86
3	12.75
4	12.76
5	11.14
6	10.98
7	9.98
8	10.42
9	12.97
10	12.95
Average	12.32

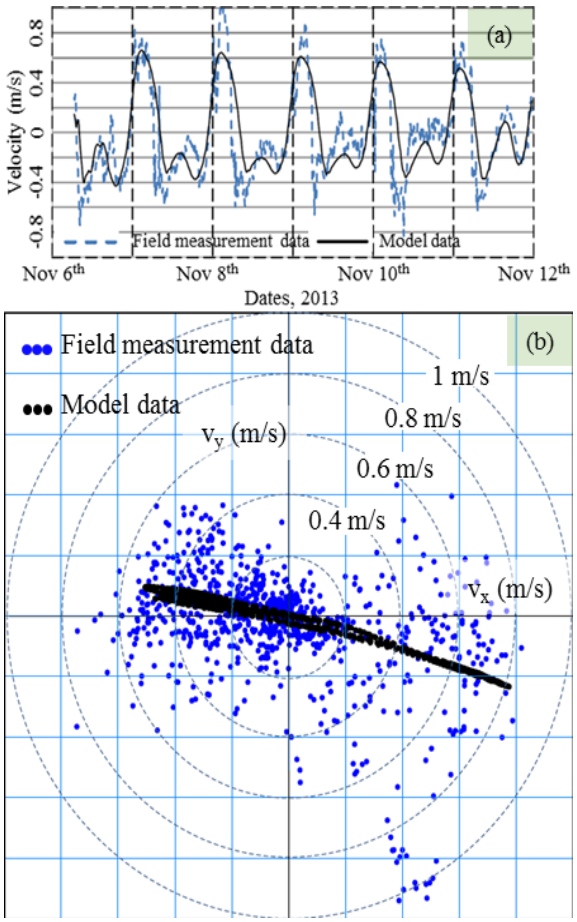

***Figure 13**. Tidal current velocity validation at Kelian Cape at layer 7*

5. Result and Analysis

5.1 Tidal Current Model

The potential site for harvesting the tidal current induced power is determined by the spatial and vertical distribution of the numerical model result. Figure 14 shows spatial views of the results of the tidal current model during the spring flood, spring ebb, neap flood, and neap ebb tides. The tidal current during spring flood and neap flood conditions results in a relatively large current velocity magnitude. From the spatial distribution analysis, three points of interest are introduced, as seen in Figure 15. They are denoted by P1, P2, and P3. Figure 16 shows the tidal current velocity scatter plot at each point. It can be seen that location P1 shows the best potential site.

Figure 16a shows that location P1 has the maximum velocity of approximately 1.4 m/s, which are twice the maximum velocities at P2 and P3. The direction of field data and the resulted model show a good correlation with the geometry of the strait.

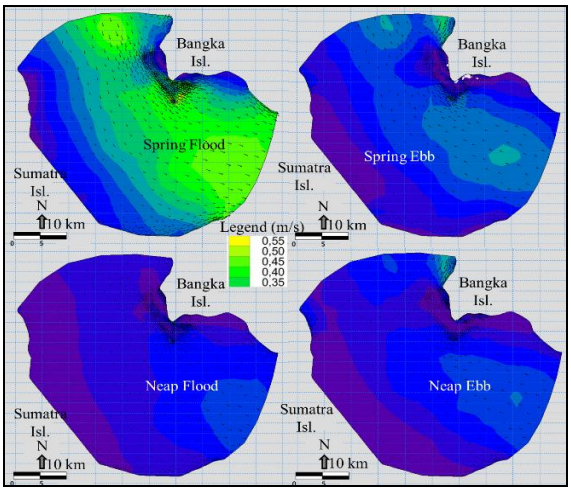

***Figure 14:** Velocity spatial distributions for various conditions*

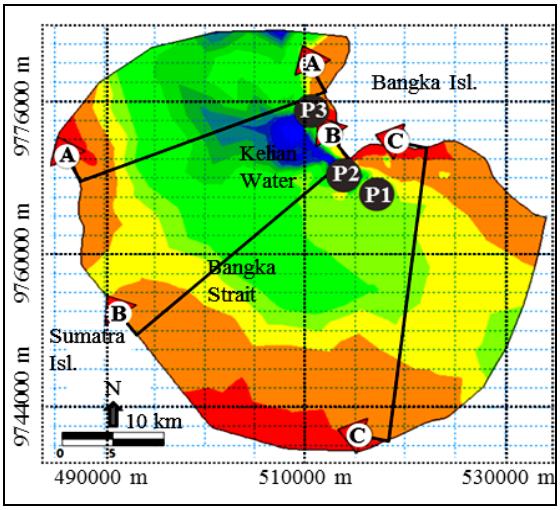

***Figure 15**. Location and cross-section marking of potential sites*

Figures 17a to 17c show the vertical distributions of velocity during spring flood conditions at the three cross-sections A–A, B–B, and C–C. The highest velocity magnitude is seen to be located in the uppermost layer. Figure 17c shows that the tidal current velocity of cross-section C–C is approximately 0.6 m/s in the uppermost layer.

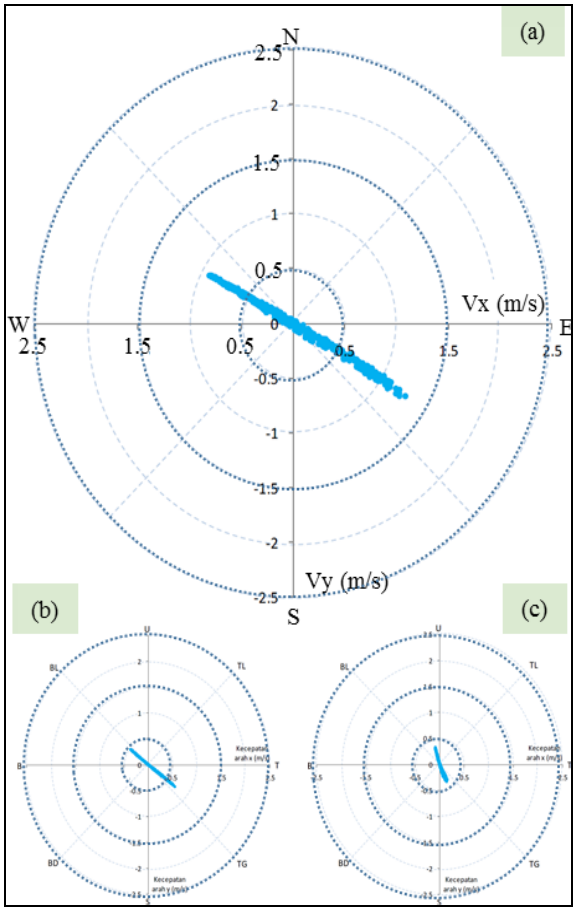

***Figure 16**. Scatter plots of tidal current at the potential site a) P1, b) P2, and c) P3*

Combining the analyses of both spatial and vertical distributions, the best potential location is near to the corner of the north inlet of Bangka Strait. The shape of the geometrical curve of the strait causes a large tidal current velocity.

5.2 Power Calculation

Energy power calculations are conducted at the potential site near the port of Muntok, at specific locations called Muntok1, Muntok2, and Muntok3, as seen in Figure 18. The depth and tidal current velocity characteristics of these potential sites (see Table 2) are used as the criteria for the selection of the turbine. The depth-averaged tidal current velocity is 0.44 m/s and the average depth is 12.48 m. The Verdant kinetic hydropower system (KHPS) is selected. The Verdant KHPS cut-in speed is 0.7 m/s, which is relatively low compared to other devices. Figure 19 illustrates the velocities for one year at Muntok3 at Layer 4, which is above the Verdant KHPS cut-in speed threshold. Verdant KHPS is also provided with good system efficiency. System efficiency consists of the efficiency of the turbine, drive train, generator, and power conditioning. The value of each efficiency and the overall system are given in Table 3 [6].

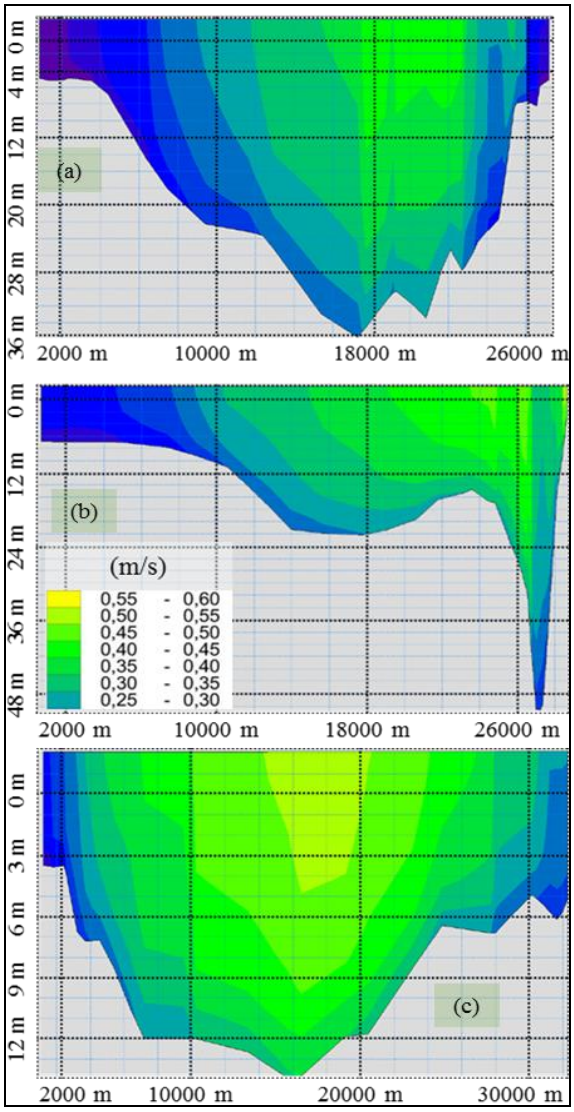

***Figure 17**. Distribution of velocity magnitudes at a) cross section A-A, b) cross section B-B, c) cross seciton C-C*

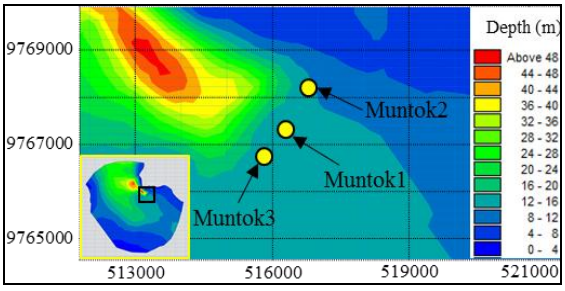

***Figure 18**. Three locations in the Muntok area (the site with the most potential)*

***Table 2**. Potential site details*

Site	Depth (m)	Average velocity (m/s)	Layer covered
Muntok1	13.4	0.44	1–6
Muntok2	11.7	0.43	1–7
Muntok3	12.4	0.45	1–7

The device is designed to be mounted on the seabed at a height of 5.5 m, which allows a minimum of 3.5 m clearance from the Lowest Low Water Level (LLWL) to ensure the safety of local people's boat navigation and other water activities. The LLWL is located 2.3 m below mean sea level (MSL). The position of the device when tidal elevation in MSL is illustrated in Figure 20. Figure 21 presents the parameter variation to help illustrate the methods of power calculation under the same conditions as Figure 20.

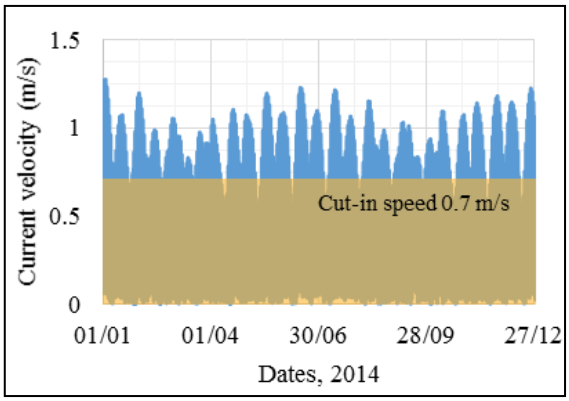

***Figure 19**. One-year tidal current output resulting from numerical model at layer 4 at Muntok3. The velocity magnitude data above the cut-in speed threshold are used in the power calculation*

***Table 3**. Turbine specifications*

Parameter	Value
Swept area	19.625 m^2
Height	5.5 m
Foundation	Mounted on seabed
Efficiency	36.1%
Cut-in speed	0.7 m/s

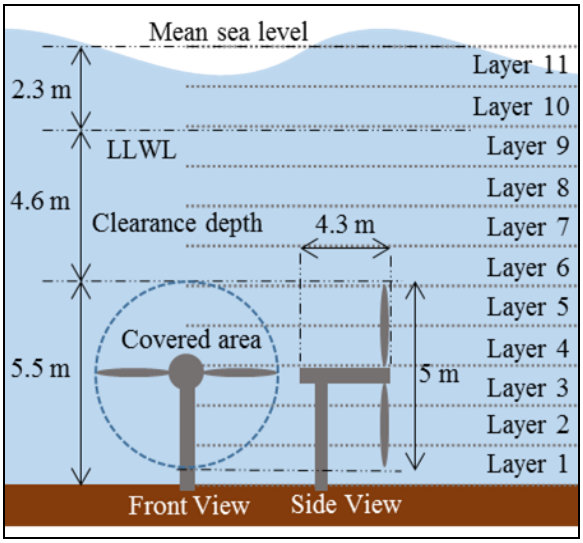

***Figure 20**. Placement of Verdant KHPS*

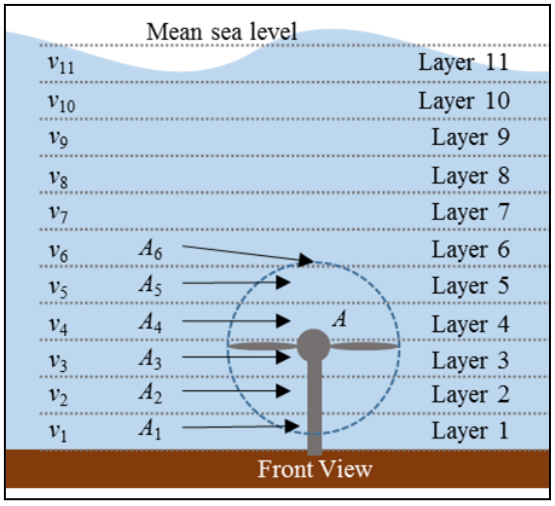

***Figure 21**. Parameter variation for Verdant KHPS operation*

The basic formula for calculating the power, P of the tidal current is given in Eq. 5, where ρ is the fluid density (1025 kg/m^3), η is the system efficiency, A is the turbine swept area, and v is the tidal current velocity. The fluid density and system efficiency are considered constant in the calculation. The swept area and tidal current velocity vary since the velocity is provided in 10 layers and there is a shift of the tidal elevation. The variation means that two power calculation methods must be performed, referred to as the average velocity based (avb) and the integrated power (ip) methods.

$$P = \frac{1}{2} \times \rho \times \eta \times A \times v^3 \quad (5)$$

5.2.1 Average Velocity Based Method

In the average velocity based (avb) method of calculating the power, it is assumed that the turbine rotates with the same velocity as the average velocity of the covered layer. The harvested power (P_{avb}) is calculated by Eq. 6. The term $\bar{v}$ is the average velocity of the covered layer. Equation 7 expresses $\bar{v}$ under the conditions as presented in Figure 21.

$$P_{avb} = \frac{1}{2} \times \rho \times \eta \times A \times \bar{v}^3 \quad (6)$$

$$\bar{v} = \frac{v_1 + v_2 + v_3 + v_4 + v_5 + v_6}{6} \quad (7)$$

5.2.2 Integrated Power

In the integrated power (ip) calculation method, it is assumed that the harvested power is a result of the integration of the generated power from each covered layer. As an example, in Figure 21 the harvested power is obtained by accumulating the generated power from layer 1 to layer 6. The harvested power from the integrated power method (P_{ip}) is given be Eq. 8. The power from the i^{th} layer (P_i) is calculated by Eq. 9, which is similar to Eq. 5. In Eq. 9, A_i is the

swept area at the i^{th} layer and v_i is the current velocity at the i^{th} layer, which is different for each layer.

$$P_{ip} = P_1 + P_2 + P_3 + P_4 + P_5 + P_6 \quad (8)$$

$$P_i = \frac{1}{2} \times \rho \times \eta \times A_i \times v_i^3 \quad (9)$$

5.2.3 Comparison

The results of sample calculations for Muntok3 on January 4th 2017, 03:00, for both methods, is presented in Table 4, which shows that the avb method yields more power than the ip method. Overall, for one year in 2014, the calculated harvested power with the avb and ip methods are 3,585.72 kWh and 3,270.18 kWh, respectively.

***Table 4**. Power calculation using average power based and integrated power methods at Muntok3 on January 4th 2014, 03:00*

		A_i (m^2)	v_i (m/s)	P_i (kW)
Integrity power method	Layer 1	1.212	0.969	0.204
	Layer 2	4.373	1.139	1.195
	Layer 3	5.282	1.220	1.776
	Layer 4	5.076	1.274	1.941
	Layer 5	3.528	1.313	1.478
	Layer 6	0.154	1.344	0.069
	Layer 7	0	1.370	0
				P_{ip} = 6.663
Average velocity based method		A = 19.625	$\bar{v}$ = 1.233	P_{avb} = 6.802

The average velocity based power method yields more power since the contributions to the harvested power of the highest and lowest covered layers are the same. With the integrated power calculation method, the lowest covered layer contributes more power since the covered swept area is bigger than at the highest covered layer. The harvested powers for all potential sites, using both calculation methods, are given in Table 5.

***Table 5**. Harvested power calculated with average velocity based power and integrated power methods*

Locations	Harvested power in 2014 (MWh)	
	Average velocity based power	Integrated power
Muntok1	3,131.69	2,957.46
Muntok2	2,349.44	2,345.78
Muntok3	3,585.72	3,270.18

another aspect which needs to be taken into account is the productivity of the device. Productivity is the percentage of the active hours to the total hours for one year. Active hours are when current velocity is bigger than the device cut-in speed. Both calculation methods result in the same productivity, 17.3%. This productivity percentage is lower than solar power usage in Indonesia, which roughly work 6 hours per day or 25% [22].

***Table 6**. Expenditure list of the tidal current power harvesting infrastructure*

No	Expenditures list	Types	Quantities	Units	Nominal	
1	Turbine fabrication	Capital	9	Turbines	IDR	13,824,744,300
2	Turbine transportation	Capital	3	Containers	IDR	114,428,400
3	Turbine installation	Capital	9	Turbines	IDR	1,853,800,200
4	Underwater cable	Capital	27	km	IDR	4,509,000,000
5	Ground cable	Capital	27	km	IDR	4,509,000,000
6	Rectifier	Capital	3	Set	IDR	901,800,000
7	Inverter	Capital	3	Set	IDR	651,300,000
8	Transformer	Capital	1	Set	IDR	100,200,000
9	Electrical equipment transportation	Capital	3	Containers	IDR	119,789,100
10	Navigation aids	Capital	1	Set	IDR	918,750,000
11	Operation	Annual	1	Set	IDR	1,147,500,000
12	Maintenance	Annual	1	Set	IDR	1,100,112,480

5.3 Project Financial Analysis

Nine Verdant KHPS turbines are deployed at the three potential sites with three turbines per site. Table 6 presents a rough estimate of the expenditures, including turbines, electrical equipment, and navigation aids, to develop the project.

The expenditure types are capital and annual cost. The capital investment needed is IDR 29,750,424,480. The investment is designed to be fully supported by bank with 10% loans rate. The annual cost is IDR 2,247,612,480. This annual cost rise follows assumed constant inflation rate of 5.97%.

The costs of installment and the annual costs are presented in Figure 22, which also presents the benefit obtained by selling the harvested power (see Table 5, integrated power) at the current price of electricity, IDR 900/kWh, which also rises following the inflation rate.

Figure 22 clearly shows that the costs and benefits are not proportional. The calculated Net Present Value (NPV) and Benefit Cost Ratio (BCR) are IDR -48,968,562,764 and 0.55, respectively, which indicates an extremely unfeasible project. To reach a positive NPV and over 1 BCR, the selling price would have to be more than IDR 74,150/kWh, which is 82 times greater than the current price.

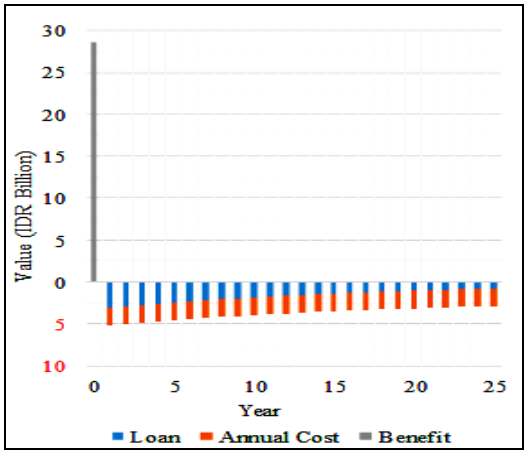

***Figure 22**. Cash flow of estimated benefits and costs*

6. Conclusions

The numerical model of Bangka Strait presents good agreement with the primary and secondary validation data, both for surface elevation validation and tidal current velocity validation. Further tidal current model analysis shows P1 as a potential location, containing the three trial sites Muntok1, Muntok2, and Muntok3. Muntok3 generates more power than the other sites according to Verdant KHPS. Further research on turbines with a lower cut-in speed is needed in order to harvest relatively smaller current velocities. However, we have discovered a potential site that has continuously available current, thus giving future hope of energy harvesting in the area around Bangka Island. The high cost of renewable energy power harvesting is still the major challenge in this case. However, the mass production and popular usage of renewable power energy will reduce the expenses, especially as fossil-based energy depletes, the competitiveness of this renewable energy will rise significantly. The same occurred in the compact disc revolution: The price of a compact disc when it was introduced in the 1980's was much higher (e.g., a compact disc and its player cost up to USD 1000), and after being popular and in high demand, the price decreased significantly.

References

[1] Metz, B., Davidson, O., Bosch, P., Dave, R. and Mayer L., "Climate change 2007 Mitigation". The Intergovernmental Panel on Climate Change, Ch. B, PP. 3-9, 2007

[2] Sugiyono, A., Anindhita, Wahid, L. M. A. and Adiarso, "Indonesia energy outlook 2016: Energy development in supporting green industry". Agency for The Assessment and Application of Technology, Ch. 2, PP. 10-30, 2016

[3] Mukhtasor, Susilohadi, Erwandi, Pandoe, W., Iswadi A., Firdaus, A. M., Prabowo, H., Sudjono, E., Prasetyo E. and Ilahude D., "Potensi energi laut Indonesia, Asosiasi Energi Laut Indonesia". Asosiasi Energi Laut Indonesia, Ch. 2, PP. 4-22, 2014

[4] Bedard, R., "EPRI survey and characterization - Tidal in stream conversion devices". Electric Power Research Institute, Ch. Appendix I, PP. 95-102, 2005

[5] Lee, S. H., Lee, S. H., Jang, K., Lee, J. and Hur, N., "A numerical study for the optimal arrangement of ocean current turbine generators in the ocean current power parks", Current Applied Physics, 10, PP. 137-141, 2010, DOI:10.1016/j.cap.2009.11.018

[6] Rahman, A. and Venugopal V., "Parametric analysis of three dimensional flow models applied to tidal energy sites in Scotland", Estuarine, Coastal, and Shelf Science, 189, PP. 17-32, 2017, DOI:10.1016/j.ecss.2017.02.027

[7] Neill, S. P., Hashemi, M. R. and Lewis, M. J., "Tidal energy leasing and tidal phasing", Renewable Energy, 85, PP. 580-587, 2016, DOI:10.1016/j.renene.2015.07.016

[8] Suryawati, S. H. et al, 2013. Kajian sosial ekonomi pengembangan dan pemanfaatan energi baru dan terbarukan di sektor kelautan dan perikanan. Laporan Akhir Penelitian. Balai Besar Penelitian Sosial Ekonomi Kelautan dan Perikanan. 2013.

[9] Ajiwibowo H., Pratama M.B., Wurjanto A., "Assessment of tidal current power potency in Kelabat Bay, Indonesia", International Journal of Engineering Technology, 9, PP. 3100-3110, 2017, DOI: 10.21817/ijet/2017/v9i4/170904089

[10] Dishidros Staff, "Tide tables of Indonesia Archipelago 2013". Dishidros, Ch. 1, PP. 174-187, 2013

[11] Dishidros Staff, "Tidal stream tables of Indonesia Archipelago 2013". Dishidros, Ch. 1, PP. 61-88, 2013

[12] Hartoko, A., Helmi, M., Sukarno, M. and Hariyadi, "Spatial tsunami wave modeling for the South Java Coastal Area, Indonesia", International Journal of Geomate, 11, PP. 2455-2460, 2016

[13] Takagi, H., Esteban, M., Mikami, T. and Fujii Daisuke, "Projection of coastal floods in 2050 Jakarta", Urban Climate, 17, PP. 135-145, 2016, DOI:10.1016/j.uclim.2016.05.003

[14] Takagi, H., Tsurudome, C., Thao, N. D., Anh, L. T., Ty, T. V. and Tri, V. P. D., "Flow intensification induced by tidal oscillations in tributaries of the Mekong River", International Journal of Safety and Security Engineering, 6, PP. 697-703, 2016, DOI:10.3178/hrl.10.21

[15] Jia, P., Wang, Q., Lu, X., Zhang, B., Li, C., Li, S., Li, S. and Wang, Y., "Simulation of the effect of an oil refining project on the water environment using the MIKE 21 model", Physics and Chemistry of the Earth, 1-10, 2017

[16] Jeyaraj, S. K. and Venugopal, V., "Assessment of tidal energy potential along The Gulf of Khambhat, Gujarat, India." Conference on

Offshore Renewable Energy, Glasgow, United Kingdom, 12-14 September, 2016, CORE 2016
[17] Work, P. A., Haas, K. A., Defne, Z. and Gay, T., "Tidal stream energy site assessment via three-dimensional model and measurements", Applied Energy, 102, PP. 510-519, 2013, DOI:10.1016/j.apenergy.2012.08.040
[18] Murray, R. O. and Gallego, A., "A modelling study of the tidal stream resource of the Pentland Firth, Scotland", Renewable Energy, 102, PP. 326-340, 2017, DOI:10.1016/j.renene.2016.10.053
[19] Gao, P., Zheng, J., Zhang, J. and Zhang, T., "Potential assessment of tidal stream energy around Hulu Island, China", Procedia Engineering, 116, PP. 871-879, 2015, DOI:10.1016/j.proeng.2015.08.376
[20] DHI Software, "MIKE 21 & MIKE 3 Flow Model FM". DHI Water & Environment, Ch. 2, PP. 3-28, 2007
[21] Novo, P. G. and Kyozuka, Y., "Field measurement and numerical study of tidal current turbulence intensity in the Kobe Strait of the Goto Islands, Nagasaki Prefecture", Journal of Marine Science and Technology, 22, PP. 335-350, 2017, DOI:10.1007/s00773-016-0414-x
[22] Suwarno, "Optimization of solar panel module positions", International Journal of Engineering Research, 6, PP. 187-189, 2017, DOI: 10.13140/RG.2.1.2660.6241